Polymer Chemistry

ROYAL SOCIETY OF CHEMISTRY

PAPER

View Article Online
View Journal | View Issue

Cite this: *Polym. Chem.*, 2023, **14**, 4589

Dispersion of ultrastable crown-ether-functionalized triphenylamine and pyrene-linked porous organic conjugated polymers with single-walled carbon nanotubes as high-performance electrodes for supercapacitors†

Mohamed Gamal Mohamed, *[a,b] Wan-Chun Chang,[a] Swetha V. Chaganti,[c,d] Santosh U. Sharma,[c,d] Jyh-Tsung Lee[c,d,e] and Shiao-Wei Kuo *[a,e]

Received 17th June 2023,
Accepted 16th September 2023

DOI: 10.1039/d3py00708a

rsc.li/polymers

We have successfully synthesized a new type of porous organic polymer (POP), called CE-Py POP, which incorporates both crown ether and pyrene using a [4 + 4] Schiff base condensation method. The CE-Py POP structure has been confirmed through various analytical techniques and has exhibited excellent thermal stability and char yield, with a T_{d10} value of 416 °C and 67 wt%, respectively. To create suitable materials for supercapacitor devices, we blended CE-Py POP with single-walled carbon nanotubes (SWCNTs) through π–π interactions to form a CE-Py POP/SWCNT nanocomposite. In galvanostatic charge–discharge (GCD) experiments, the CE-Py POP/SWCNT nanocomposite exhibited an impressive specific capacitance value reaching 346 F g^{-1} and demonstrated exceptional capacitance retention, maintaining 97.6% of its original capacitance even after more than 2000 cycles.

Introduction

The ongoing utilization of finite resources and the continuous exhaustion of fossil fuels have resulted in environmental disasters, such as climate change, underscoring the pressing requirement to transition to sustainable sources of energy.[1–4] In this context, supercapacitors (SCs) have emerged as promising devices of energy storage technology thanks to their rapid charging capability, high power density, eco-friendly characteristics, and long lifespan.[5] Supercapacitors are energy storage devices that possess qualities resembling both batteries and conventional capacitors. Their distinct design and composition enable swift energy storage and release, presenting an appealing substitute for conventional batteries and capacitors across various applications.[6,7] Multiple studies have reported that the energy storage mechanism in supercapacitors relies on electrostatic interactions between the electrolyte ions and the carbon electrodes.[1,8–10] The selection of electrode materials plays a significant role in determining the electrochemical performance and mechanism of supercapacitors. Organic materials, including conducting polymers (CPs) and porous organic polymers (POPs), hold distinct advantages over inorganic and inorganic–organic hybrid materials due to their facile chemical modification, cost-effective production, and adaptable functionalities.[1–4] Nonetheless, inherent limitations such as restricted solubility, modest capacitance in their pure state, inadequate electrical conductivity, and modest electrochemical stability have hindered their utilization as electrode materials.[1] Consequently, there is a pressing demand for the development of robust electrode materials to enhance the performance of supercapacitors (SCs). Untreated CPs usually exhibit sub-par bulk conductivity, which poses challenges when they are employed for energy storage applications like batteries and supercapacitors. This often necessitates the incorporation of substantial additives, such as carbon. Paradoxically, even CP materials with substantial intrinsic charge storage capabilities may not lead to proportionate gains in overall storage capacity for the final device. Researchers have directed their attention toward the advancement of electrode material components and topologies in order to circumvent the limitations associated with supercapacitors[11–14] Porous organic polymers (POPs), such as CMPs, COFs, and CNTs, have garnered significant attention

[a]*Department of Materials and Optoelectronic Science, Center for Functional Polymers and Supramolecular Materials, National Sun Yat-Sen University, Kaohsiung 804, Taiwan. E-mail: mgamal.eldin12@yahoo.com*
[b]*Department of Chemistry, Faculty of Science, Assiut University, Assiut 71515, Egypt*
[c]*Department of Chemistry, National Sun Yat-Sen University, Kaohsiung80424, Taiwan*
[d]*International PhD Program for Science, National Sun Yat-sen University, Kaohsiung 80424, Taiwan*
[e]*Department of Medicinal and Applied Chemistry, Kaohsiung Medical University, Kaohsiung 807, Taiwan. E-mail: kuosw@faculty.nsysu.edu.tw*
† Electronic supplementary information (ESI) available. See DOI: https://doi.org/10.1039/d3py00708a

as electrode materials for electric double-layer capacitors (EDLCs). The incorporation of these materials brings forth numerous advantages, such as affordability, chemical stability, and widespread availability. These factors collectively contribute to enhancing the overall performance of supercapacitors.[15–17] POPs are characterized by a multidimensional porous network interconnected by covalent bonds.[18]

The extensive range of building blocks and reaction pathways available allows for the creation of POP materials with diverse architectures and a wide range of characteristics.[19] Materials made of POPs have a number of notable qualities, including ease of fabrication, large surface area, a variety of porosities, outstanding thermal stability, a wide light spectrum, and advantageous optoelectronic capabilities.[20–22] POPs are therefore suitable for a wide range of applications, including energy storage, photoredox catalysis, gas separation, ion detection, and H_2 production.[23–27] However, supercapacitors have a critical limitation that severely restricts their potential uses: their low energy density. As a result, significant research has been devoted to investigating strategies like electrode nanostructuring to increase the energy density of supercapacitors.[28–30] The combination of CMPs with other conductive carbon materials like graphene and carbon nanotubes (CNTs) presents a more effective strategy for enhancing the conductivity of CMPs, thereby elevating their electrochemical performance.[31,32] Notably, CNTs offer an expansive surface area that is conducive to charge storage, making them excellent candidates for supercapacitor electrode materials. Their superior electrical conductivity, surpassing that of other carbon-based materials, facilitates rapid charging and discharging processes. Consequently, we propose that the synergistic integration of the porous nature of CMPs with the conductivity of CNTs holds greater promise for enhancing electrode materials compared to their individual deployment. It has been demonstrated that SWCNTs considerably enhance the electrochemical performance of supercapacitors. The special characteristics of SWCNTs, such as their distinct structure, high conductivity of electricity, and superior S_{BET}, may be responsible for this improvement. These characteristics enable the quick and effective movement of electrons as well as ions inside electrode materials, enhancing the overall performance of supercapacitors.[1,4,33–38] Additionally, SWCNTs can increase the mechanical stability and hardness of electrode materials, making them highly desirable for outstanding energy storage device performance.[1,31,39] Crown ethers (CEs) have been employed as materials for electrodes in supercapacitors because of their unique properties. The electron-rich cavities included in CEs may enhance the capacitive characteristics of electrodes, thereby enhancing the electrochemical performance of the supercapacitor.[40] Additionally, due to the inherent affinity of CEs for cations, the electrode may become more selective towards certain ions, increasing the efficiency and cycling stability of the supercapacitor.[41,42] In this study, the [4 + 4] Schiff base condensation approach was utilized to successfully synthesize a novel porous organic polymer (POP) named CE-Py POP by combining crown ether and pyrene.

Rigorous analytical methods were employed to confirm the structure of CE-Py POP, revealing its impressive char yield and thermal stability. By leveraging π–π interactions, SWCNTs were integrated with CE-Py POP to create materials suitable for supercapacitor devices, resulting in the formation of a CE-Py POP/SWCNT nanocomposite. Remarkably, the CE-Py POP/SWCNT nanocomposite exhibited exceptional capacitance retention of 97.6% and a noteworthy specific capacitance value of up to 346 F g^{-1} as demonstrated through galvanostatic charge–discharge (GCD) studies.

Experimental

Materials

Hydrazine monohydrate ($NH_2NH_2{\cdot}H_2O$), acetic acid (AcOH), absolute ethanol (EtOH), 4-formylphenylboronic acid [4-$CHOPhB(OH)_2$], MeOH, and DMF were bought from Sigma-Aldrich. Pd/C (10 wt%), 1,4-dioxane (DO), and dichloromethane (CH_2Cl_2, DCM) were purchased from Acros. Potassium carbonate (K_2CO_3, 99.99%) and 1-fluoro-4-nitrobenzene were obtained from Alfa Aesar. SWCNTs were ordered from the Center of Biochemistry Technology. *trans*-Di(aminobenzo)[18]crown-6 (CE-$2NH_2$) and 1,3,6,8-tetrabromopyrene (Py-Br_4) were synthesized using previously reported procedures.[40,43]

Synthesis of dibenzo-crown ether-$4NO_2$ (CE-$4NO_2$)

A mixture of CE-$2NH_2$ (1 g, 2.56 mmol), 1-fluoro-4-nitrobenzene (1.63 mL, 15.38 mmol), K_2CO_3 (6.37 g, 46.09 mmol), Cu (0.033 g) and DMF (30 mL) was heated and stirred at 110 °C for 24 hours (under N_2). Following the reaction, the mixture underwent filtration to remove the solid, and subsequently, the DMF solvent was evaporated, resulting in the formation of a viscous brown solid. The brown solid was then dissolved in DCM and added dropwise into methanol to obtain CE-$4NO_2$ as a brown powder.

Synthesis of dibenzo-crown ether-$4NH_2$ (CE-$4NH_2$)

A mixture of CE-$4NO_2$ (1 g, 1.14 mmol), Pd/C (1.63 mL, 6.86 mmol), DO (40 mL), and EtOH (20 mL) was stirred at 90 °C for 1 hour. After the duration of one hour, a gentle addition of 1.89 mL (38.96 mmol) of $NH_2NH_2{\cdot}H_2O$ was made to the reaction solution, which was subsequently refluxed at 90 °C for a period of two days. The resulting mixture was subjected to filtration to eliminate any unreacted Pd/C, followed by evaporation of the solvent under reduced pressure. This process led to the formation of CE-$4NH_2$ as a white powder. Finally, water was used to wash the white powder to make it pure.

Synthesis of Py-4CHO

A mixture of Py-Br_4 (1.00 g, 1.93 mmol), 4-$CHOPhB(OH)_2$ (1.74 g, 11.6 mmol), $Pd(PPh_3)_4$ (0.12 g, 0.10 mmol), and K_2CO_3 (2.1 g, 15 mmol) was stirred in 30 mL of 1,4-dioxane under a nitrogen atmosphere at a temperature of 85 °C for a duration

of 72 h. An ice-and-concentrated hydrochloric acid solution was added to the resultant suspension, which had a yellow appearance. The yellow material was then extracted with $CHCl_3$ after being filtered and washed three times with 2 M HCl and H_2O The resulting product was then dried and subjected to recrystallization from hot $CHCl_3$, resulting in the formation of Py-4CHO as a bright yellow powder (yield: 70%). FTIR (cm^{-1}): 3063 (C–H stretching for the Py unit and aryl units), 1697 (C=O), and 1599 (C=C).

Synthesis of CE-Py POP

A series of freeze–pump cycles were conducted on Pyrex tubes containing CE-$4NH_2$ (100 mg, 0.13 mmol), Py-4CHO (81 mg, 0.13 mmol), DO (5 mL), mesitylene (5 mL) and 1 mL of AcOH (6 M). The tube was subjected to freezing in a liquid nitrogen bath. Subsequently, the solution was heated at 90 °C for a duration of 72 hours. The mixture underwent filtration and was subsequently subjected to a purification process involving THF, DI water, MeOH, and acetone. This purification procedure yielded brown CE-Py POP powder with an 82% overall yield.

Preparation of the CE-Py POP/SWCNT nanocomposite

In a tube, CE-Py POP (2 mg) and SWCNTs (2 mg) were mixed in methanol (2 mL) and stirred for 1 day. After evaporating the methanol, and to prepare the CE-Py POP/SWCNT nanocomposite, the remaining material was subjected to a 24-hour baking process in an oven.

Results and discussion

Synthesis of the CE-$4NH_2$ monomer

Previously, we successfully synthesized dibenzo-crown ether-$2NH_2$ (CE-$2NH_2$) with high purity and high yield.[43] Here, CE-$2NH_2$ was reacted with 1-fluoro-4-nitrobenzene in the presence of K_2CO_3 and Cu to give dibenzo-crown ether-$4NO_2$ (CE-$4NO_2$) as a brown powder. Dibenzo-crown ether-$4NH_2$ (CE-$4NH_2$) as a gray powder was synthesized by employing a reduction reaction of CE-$4NO_2$ using $NH_2NH_2{\cdot}H_2O$ in the presence of 10 wt% Pd/C in absolute ethanol (EtOH) with the addition of DO as a co-solvent [Fig. 1(a)]. The FTIR spectrum of each compound obtained at room temperature is shown in Fig. 1(b). FTIR signals are visible in the profile of CE-$2NH_2$ at 3429 and 3357 cm^{-1}, representing symmetric and asymmetric N–H stretching, respectively. The FTIR profile of CE-$4NO_2$ has signals at 1514 and 1342 cm^{-1} representing NO_2 stretching. The FTIR spectrum of CE-$4NH_2$ has signals at 3439 and 3356 cm^{-1}, also representing N–H stretching, and all compounds exhibit absorption at *ca.* 1135 cm^{-1} due to the ether unit of the CE. In order to confirm the chemical structures of the synthesized compounds, we employed NMR spectroscopy along with FTIR spectroscopy, both performed at room temp-

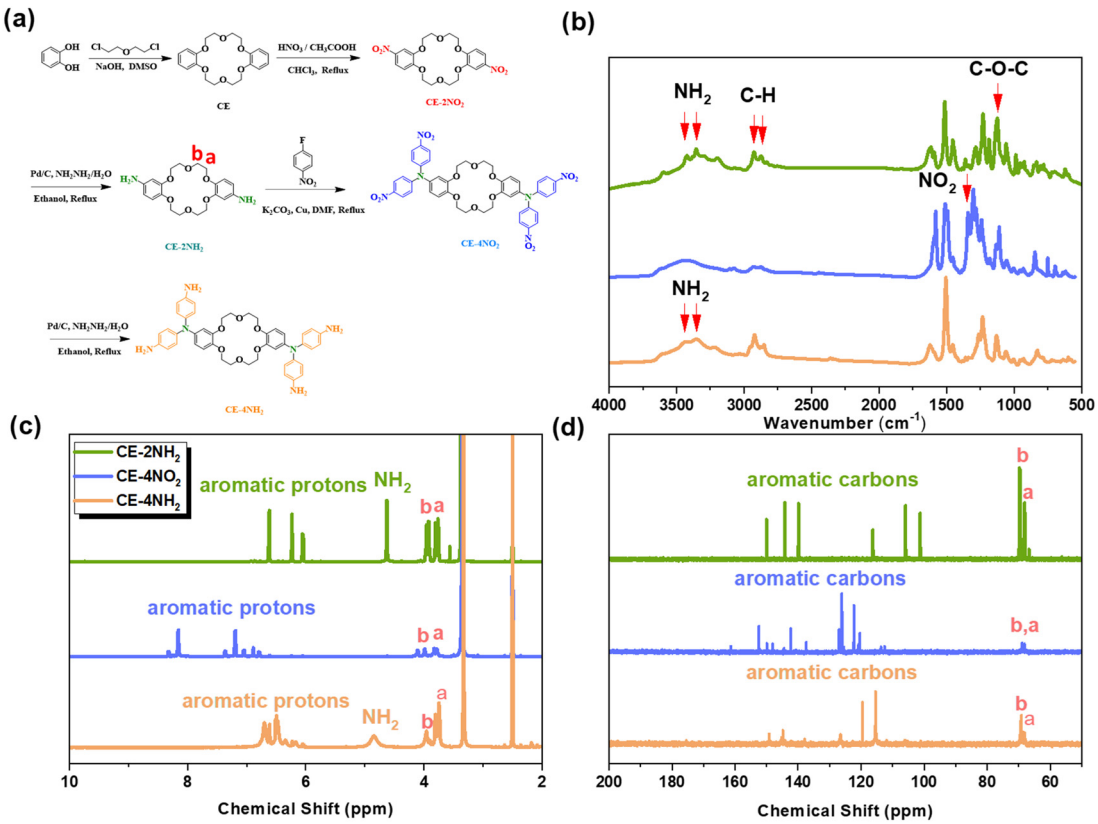

Fig. 1 (a) Synthesis of CE-$4NH_2$ from CE-$2NH_2$ and CE-$4NO_2$ and their corresponding (b) FTIR, (c) ^{1}H NMR, and (d) ^{13}C NMR spectra.

erature, and the ^{1}H and ^{13}C NMR spectra are displayed in Fig. 1(c) and (d), respectively. The ^{1}H NMR pattern of CE-2NH_2 has signals for the aryl ring, NH_2, and OCH_2 at 6.65–6.01, 4.63, and 3.99–3.73 ppm, respectively. The aromatic ring and OCH_2 exhibit peaks in the ^{1}H NMR profile of CE-4NO_2, respectively, at 8.52–6.81 ppm and 4.11–3.76 ppm, while the signal for the NH_2 unit at 4.63 ppm is totally absent. Upon reduction, the ^{1}H NMR spectrum of CE-4NH_2 exhibited distinct signals corresponding to the aromatic ring protons (6.76–6.04 ppm), NH_2 protons (4.85 ppm), and OCH_2 protons (3.93–3.75 ppm). The ^{13}C NMR profile of CE-2NH_2 displayed peaks for the carbon nuclei of the aromatic ring and OCH_2 units at 150.15–101.11 ppm and 69.93–66.85 ppm, respectively. In the ^{13}C NMR spectrum of CE-4NO_2, the carbon nuclei associated with the aromatic units were observed in the range of 152.47–112.4 ppm, while the carbon nuclei corresponding to the OCH_2 units were detected in the range of 68.67–67.60 ppm. After the reduction process, the ^{13}C NMR spectrum of CE-4NH_2 revealed signals for the aromatic units within the range of 149.33–115.38 ppm, while the carbon nuclei of the OCH_2 units exhibited signals within the range of 69.43–67.85 ppm. As a consequence, every characterization result supported the exceptional purity of the CE-4NH_2 monomer.

Synthesis and characterization of CE-Py POP

We prepared CE-Py POP through a Schiff base condensation reaction of Py-4CHO with CE-4NH_2 [Fig. 2(a)]. Fig. 2(b) shows the FTIR peaks of CE-4NH_2, Py-4CHO, and CE-Py POPs at ambient temperature. For C=N and C–O–C units, the FTIR pattern of CE-Py POP revealed absorption signatures at 1625 and 1130 cm^{-1}. Moreover, after the Schiff base condensation reaction, the absorption signal of the CE-4NH_2 monomer for the NH_2 group at 3429 and 3357 cm^{-1} disappeared, and the absorption signal of the Py-4CHO monomer for the C=O group at 1701 cm^{-1} decreased. As shown in Fig. 2(c), the solid-state ^{13}C NMR (ssNMR) spectrum for insoluble CE-Py POP was also used for structure identification.

The aromatic ring carbon nuclei and OCH_2 exhibited signals in the ssNMR pattern of CE-Py POP at 145.12–121.61 ppm and 69.97–67.42 ppm, respectively. As shown in Fig. 2(d), we used TGA to compare the thermal stability of CE-4NH_2 and Py-4CHO monomers with that of CE-Py POP in a nitrogen environment at 20 °C min^{-1}. The values of T_{d10} for CE-4NH_2 and Py-4CHO monomers were 292 and 326 °C, respectively; the values of the char yield for CE-4NH_2 and Py-4CHO monomers were 28 and 20 wt%, respectively. The values of T_{d10} and char yield for CE-Py POP were enhanced

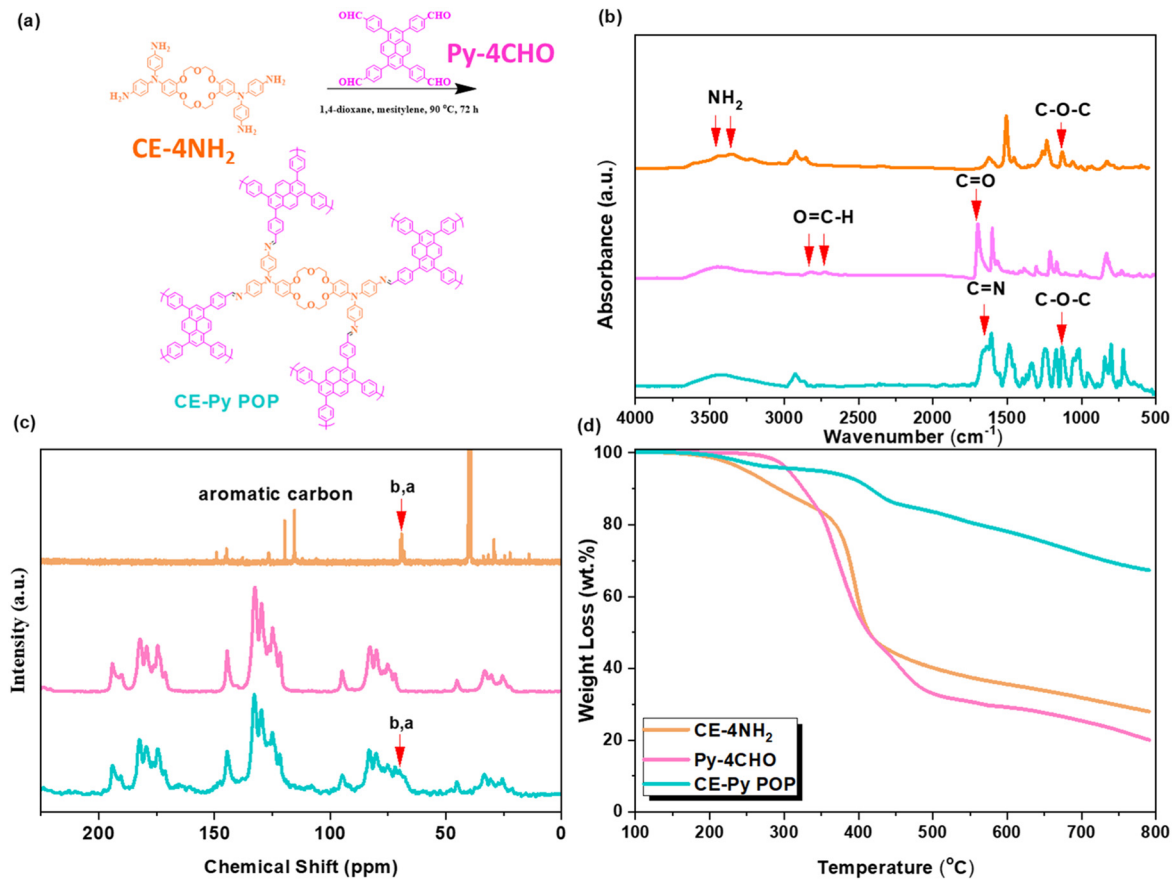

Fig. 2 (a) Synthesis of CE-Py POP from CE-4NH_2 and Py-4CHO. (b–d) Results from their corresponding analyses: (b) FTIR spectra, (c) ^{13}C solid-state NMR spectra, and (d) TGA traces.

to 416 °C and 67 wt%, respectively, after the Schiff base condensation process. This demonstrates enhanced thermal stability and the formation of highly interconnected networks. We measured the N_2 adsorption/desorption isotherms and pore size distribution of CE-Py POP at 77 K [Fig. 3(a) and (b)]. According to the definition of IUPAC, CE-Py POP exhibited type III adsorption/desorption isotherms, and the specific surface area and total pore volume were 28 $m^2\ g^{-1}$ and 0.2 $cm^3\ g^{-1}$, respectively. These results are close to those of our and other groups' previous studies of crown ether (CE)-based POPs, which reported specific surface area values of 21, 11, 33, and 47 $m^2\ g^{-1}$, respectively.[40,44,45] The pore size distribution result showed that the CE-Py POP had microporous and mesoporous characteristics in the range of 1.89–4.86 nm. We also used SEM and HR-TEM to identify the surface morphology of CE-Py POP [Fig. 3(c) and (d)]. The SEM image results for CE-Py POP illustrated the formation of rod-shaped irregular structures, and amorphous porous characteristics could be observed in the measurement results of TEM. SEM–EDS measurements also corroborated the existence of carbon (C), nitrogen (N), and oxygen (O) atoms within the CE-Py POP structure [Fig. S1†]. As shown in Fig. 4(a), CE-Py POP (2 mg) and SWCNTs (2 mg) were mixed in methanol (2 mL) and stirred for 1 day. The remaining material was baked in an oven for 24 hours after the methanol had been evaporated to produce a CE-Py POP/SWCNT nanocomposite.

TGA analyses were used to compare the thermal stabilities of CE-Py POP and CE-Py POP/SWCNT nanocomposites in a nitrogen environment at 20 °C min^{-1}. After combining with SWCNTs, the T_{d10} and char yield values for the CE-Py POP/SWCNT nanocomposite increased to 511 °C and 79 wt%, respectively. The values for T_{d10} and char yield for the CE-Py POP were 416 °C and 67 wt%, respectively, confirming that the addition of SWCNTs can improve the thermal stability of the material. The enhanced thermal stability within CE-Py-POP/SWCNT nanocomposites might stem from the physical barrier effect exerted by dispersed carbon nanotubes (CNTs), which hinder the movement of volatile decomposition products during thermal decomposition. Fig. 4(c) and (d) display the TEM images of SWCNTs and the CE-Py POP/SWCNT nanocomposite, and as shown in Fig. 4 (c1), pure SWCNTs mixed with methanol produced an aggregation phenomenon, which could be confirmed from TEM [Fig. 4(c)]. However, when CE-Py POP was added to aggregated SWCNTs, the CE-Py POP/SWCNT complexes dissolved [Fig. 4(d1)], and the CNTs were significantly dispersed throughout the CE-Py POP matrix due to the π–π stacking interaction between the CNTs and

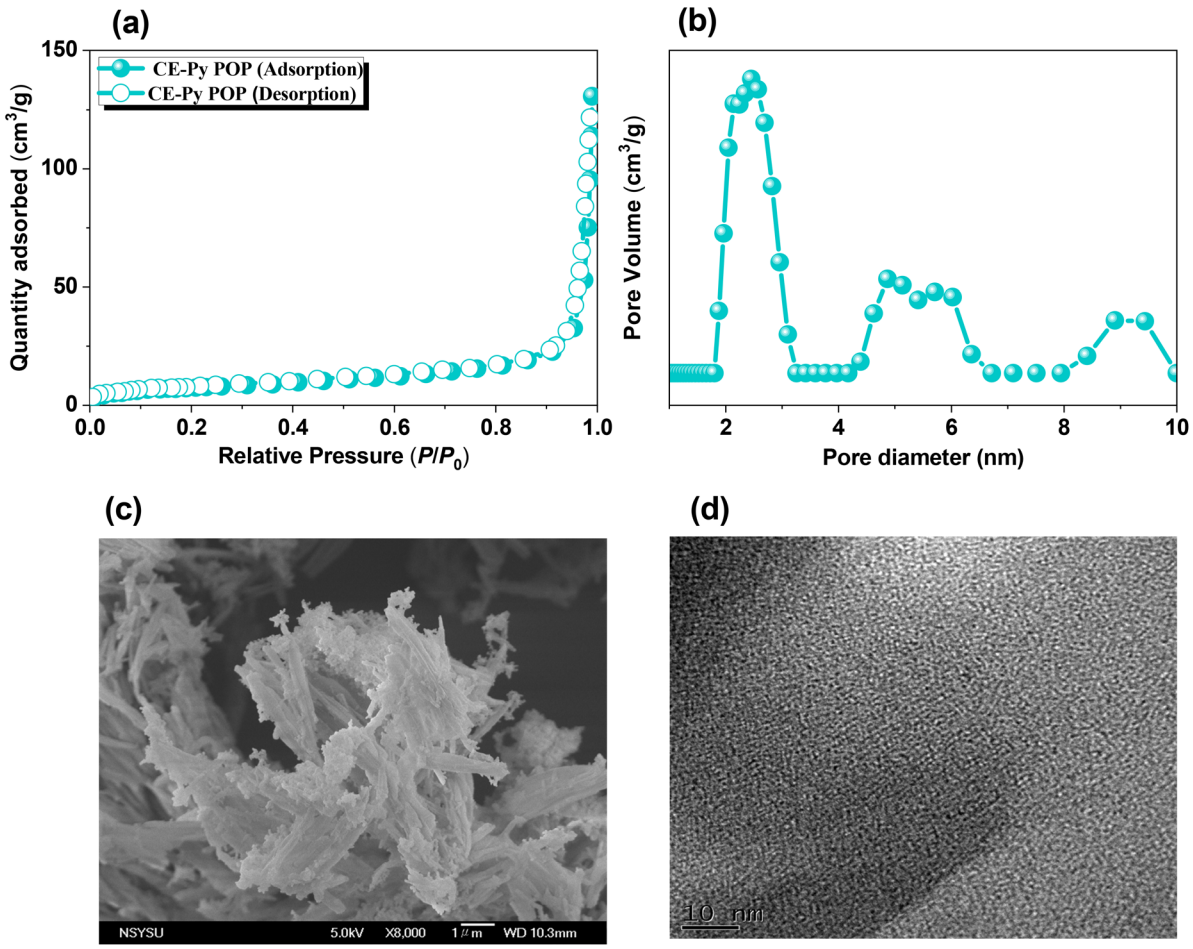

Fig. 3 (a) N_2 adsorption/desorption isotherms, (b) pore size distributions, (c) SEM image, and (d) TEM image of the CE-Py POP.

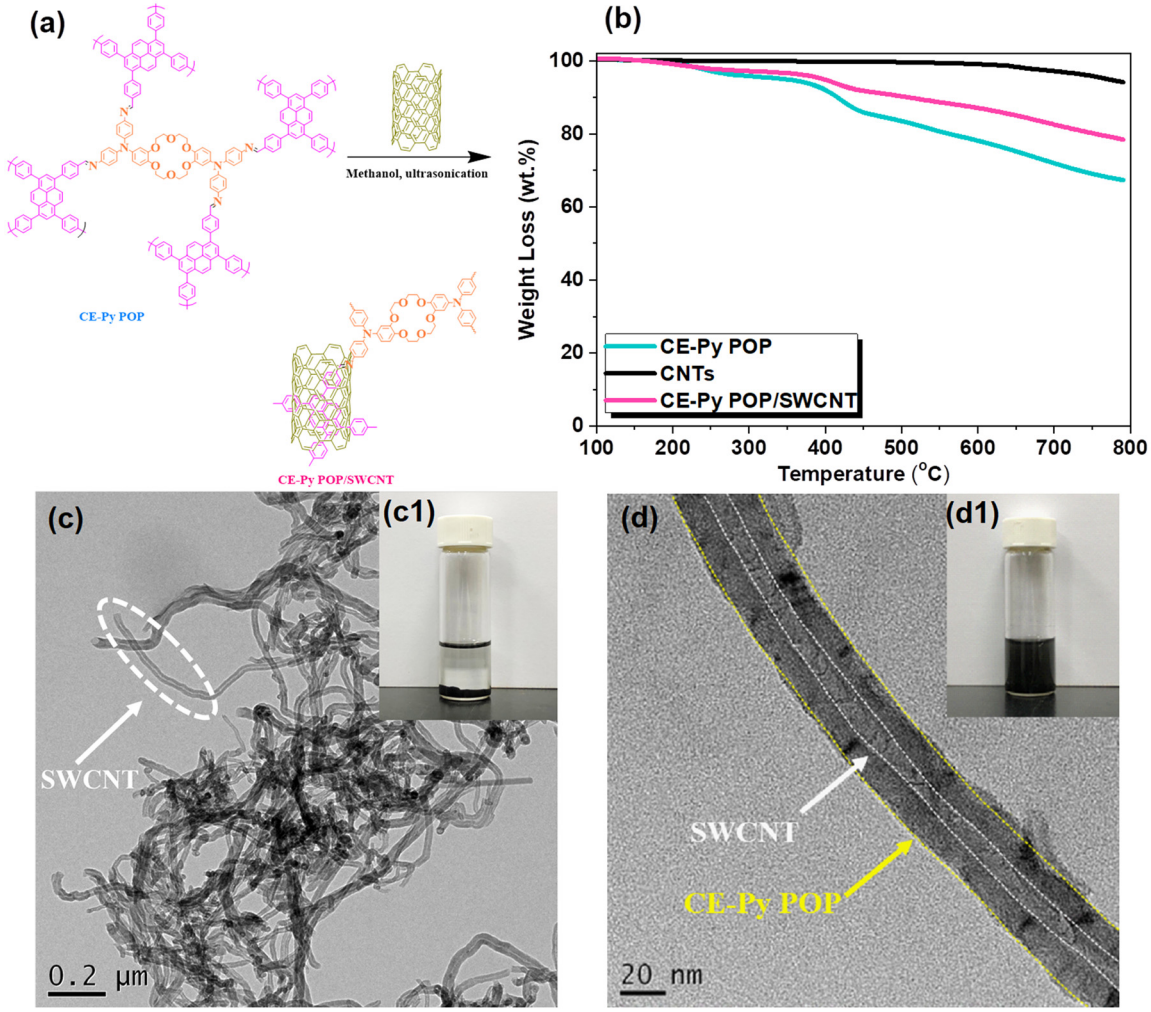

Fig. 4 (a) Synthetic route for the preparation of the CE-Py POP/SWCNT nanocomposite. (b) TGA analyses of the CE-Py POP/SWCNT nanocomposite. (c and d) TEM images of (c) pure SWCNT and (d) the CE-Py POP/SWCNT nanocomposite. Insets show photographs of pure SWCNTs (c1) and the CE-Py POP/SWCNT nanocomposite (d1) in methanol.

the CE-Py POP [Fig. 4(d)]. We conducted measurements of N_2 adsorption/desorption isotherms and analyzed the pore size distribution for both SWCNT and CE-Py POP/SWCNT samples at a temperature of 77 K, as depicted in Fig. S2.† According to the IUPAC classification, the N_2 uptake profiles of SWCNTs exhibited a type I isotherm, while those of CE-Py POP/SWCNTs displayed a type III isotherm. Notably, the specific surface area and total pore volume were observed to be 130 $m^2\ g^{-1}$ and 0.74 $cm^3\ g^{-1}$, respectively, for SWCNTs, and 15 $m^2\ g^{-1}$ and 0.14 $cm^3\ g^{-1}$, respectively, for CE-Py POP/SWCNTs. In terms of pore dimensions, the pore sizes for SWCNTs ranged between 1.19 and 8.82 nm, while those for CE-Py POP/SWCNTs were within the range of 2.33 to 5.72 nm.

Electrochemical performance of CE-Py POP and CE-Py POP/SWCNT nanocomposite

Galvanostatic charge–discharge (GCD) and cyclic voltammetry (CV) measurements were performed in 1 M KOH aqueous solution to evaluate the electrochemical performance of these compounds. Fig. 5(a) and (b) present the CV curves of CE-Py POP and the CE-Py POP/SWCNT nanocomposite. The potential window was set between −1.0 V and 0.0 V (*vs.* Hg/HgO). The electrode stability and capacitance from electric double-layer capacitors (EDLCs) were demonstrated by the distinctive rectangular humped shapes observed for both electrodes, which remained consistent throughout the scan-sweeping process[34,46,47] The rectangular morphologies with distinct humps are attributed to the reversible radical redox reactions occurring during charge and discharge operations. These reactions primarily involved electron-rich phenyl rings and nitrogen heteroatoms within the material. The pseudocapacitance of these two electrodes may be attributed to nitrogen abundance, which paved the way for efficient electron transmission by improving contact with the electrolyte.[1,48] The significant rate capability and easy kinetics of these compounds are highlighted by the CV curves. Additionally, the GCD of CE-Py POP and CE-Py POP/SWCNT were examined [Fig. 5(c and d)]. The GCD profiles of all compounds have a bent-triangular structure, which implies pseudocapacitive and EDLC features. The

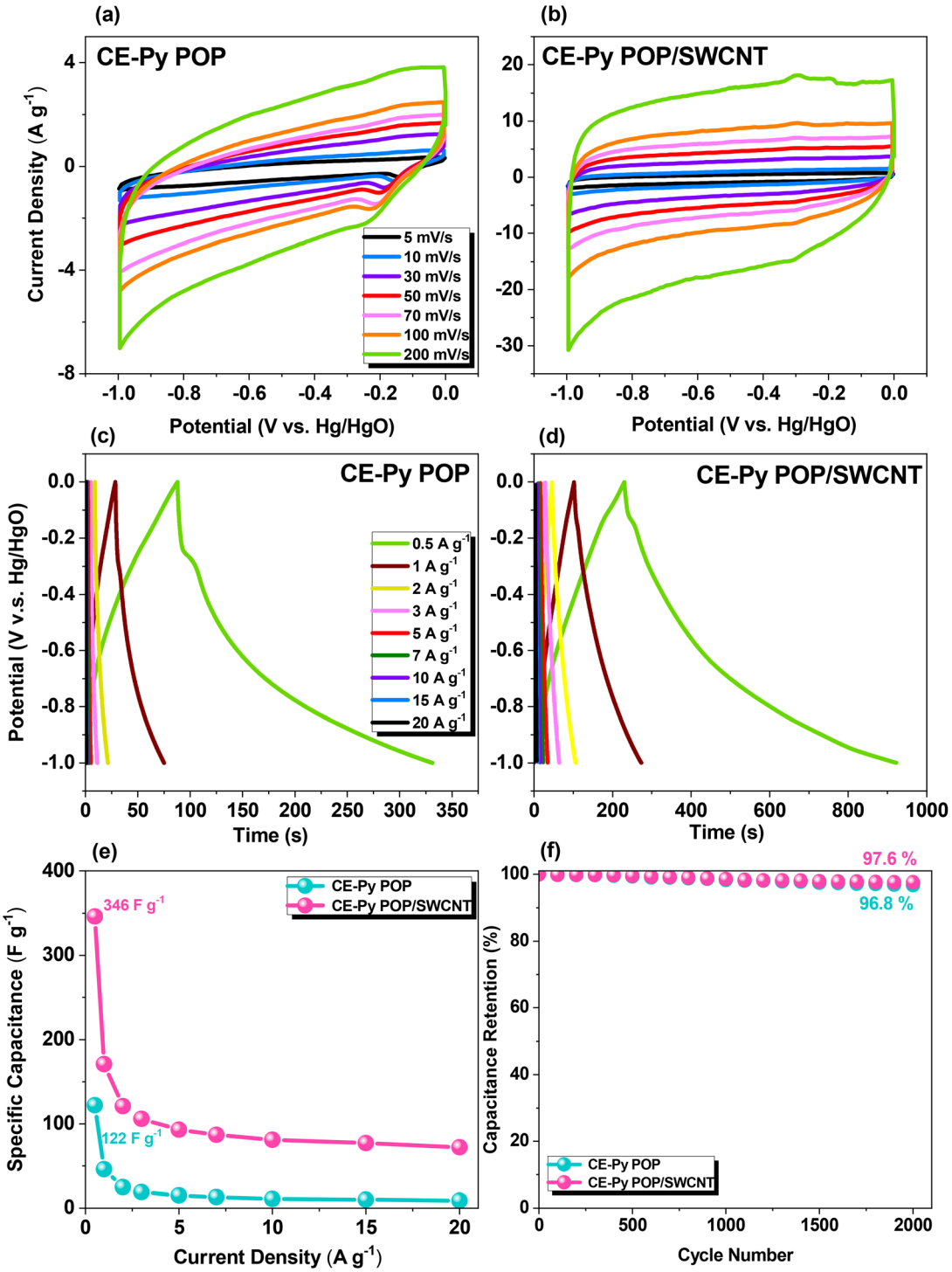

Fig. 5 (a and b) CV and (c and d) GCD profiles of (a–c) CE-Py POP and (b–d) the CE-Py POP/SWCNT nanocomposite. (e) Specific capacitance profiles measured at various current densities and (f) stability of CE-Py POP and the CE-Py POP/SWCNT nanocomposite.

presence of nitrogen atoms in the molecules could be utilized to elucidate the bent structure. Moreover, upon incorporating SWCNTs, the CE-Py POP/SWCNT nanocomposite exhibited an even longer discharge time, indicating higher capacitance. Fig. 5(e) shows the specific capacitance as measured data; the capacitance of CE-Py POP and the CE-Py POP/SWCNT nanocomposite was 122 and 346 F g^{-1}, respectively, measured at 0.5 A g^{-1}. As we are aware, SWCNTs exhibit exceptional conductivity within matrices, proving invaluable in scenarios where conductivity poses a challenge, as observed in porous organic polymers. The results from galvanostatic analyses vividly demonstrate that employing the CE-POP as an electrode yields a

specific capacity of 122 F g^{-1}. Remarkably, upon integrating SWCNTs into the CE-Py POP composites, the specific capacity experiences a substantial boost, soaring to 346 F g^{-1}. This unequivocally underscores the pivotal role played by SWCNTs within the electrode matrix alongside porous polymers. Moreover, we have conducted an assessment of the electrochemical performance of pristine SWCNTs, as presented in Fig. S3.† Notably, SWCNTs exhibit the potential to offer specific capacity values surpassing 101 F g^{-1}, coupled with their inherent conductivity enhancement, which underscores their fundamental significance. The capacitance of the CE-Py POP/SWCNT nanocomposite was three times greater than that of CE-Py POP. Additionally, the porous shape of SWCNTs offered diffusion channels and more effective electrolyte ion transport, which enhanced capacitance. The specific capacitance of both electrodes had been seen to drop with an increase in current densities. The contact between the active center of the electrode on the surface and the electrolyte diminishes as the current density rises, lowering the specific capacitance.[49,50] The cycling stability and capacity retention of these two electrodes were examined over 2000 cycles, with capacity retentions of 96.8% and 97.6% for CE-Py POP and the CE-Py POP/SWCNT nanocomposite, respectively. Since the hydrophilic properties of the CNT surface enable pathways for easy access to electrolyte ions, rapid mass movement and improved electrochemical performance could arise from enrichment with pyrene. The improved performance of the CE-Py POP/SWCNT nanocomposite can be attributed to its specific structure. The arrangement of the pyrene molecule's benzene rings forms a stacking structure with the CNTs. This structure is conducive to enhanced electrochemical activity and conductivity, as it facilitates electron dispersion. Additionally, the stacking arrangement increases the porosity of the nanocomposite, which helps in accommodating the electrolyte and mitigating its effects.[1,16] The energy density values for CE-Py POP and CE-Py POP/SWCNT were 16.94 W kg^{-1} and 48.05 W kg^{-1}, respectively, at a power density of 250 W h kg^{-1}, as illustrated in Fig. S4.† In addition to the two-electrode performances of these compounds, we built a symmetric supercapacitor coin cell as part of our assessment of their practical usage. To assemble the coin cell (Fig. 6(d)), the components included a bottom cover, a top cover, a metal spring, a separator, an anode, a cathode, and an electrolyte from a CR2032 coin cell. Our material was utilized as both the cathode and anode in order to create a symmetric supercapacitor. The slurry, prepared following the recommended

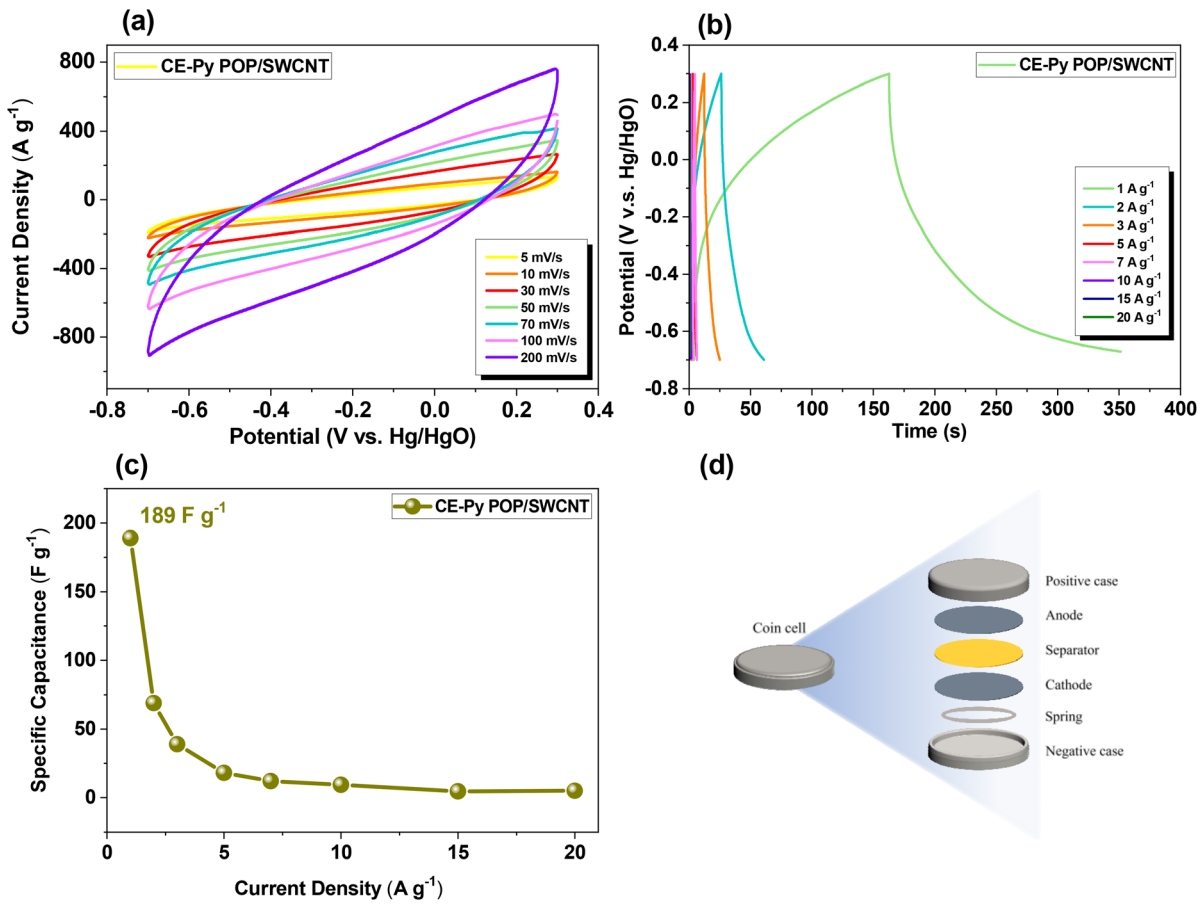

Fig. 6 (a) CV and (b) GCD profiles of the CE-Py POP/SWCNT nanocomposite. (c) Specific capacitance profiles of the CE-Py POP/SWCNT nanocomposite recorded at various current densities. (d) Schematic diagram of the CE-Py POP/SWCNT nanocomposite coin cell configuration.

ratio provided in the article, was then coated onto carbon paper. For the electrolyte, a Selemion AMV membrane and an aqueous solution of 1.0 M KOH were employed. All electrochemical tests were conducted between −0.7 V and 0.3 V potentials and at varied scan rates between 5 and 200 mV s^{-1}. Fig. 6(a) represents the cyclic voltammetry profiles of symmetric coin cells for supercapacitors measured at scan rates of 5 to 200 mV s^{-1} for the CE-Py POP/SWCNT nanocomposite. The EDLC and pseudocapacitive properties of the electrode materials contributed to giving these CV curves their essentially rectangular shape. As we increased the scan speeds from lower to higher, the current density increased, highlighting the improved stability and improved kinetics of these electrode materials.[51–57] The GCD curves were evaluated at different current densities and are shown in Fig. 6(b). These GCD curves exhibited triangular shapes with slight bends, which indicated EDLC and pseudocapacitive characteristics.[58–61] The specific capacitance of the CE-Py POP/SWCNT nanocomposite was calculated as 189 F g^{-1} at 1 A g^{-1} [Fig. 6(c)]. A schematic diagram of the CE-Py POP/SWCNT nanocomposite coin cell configuration is shown in Fig. 6(d). Thus, this porous organic polymer demonstrates existing potential as electrode material for real-life energy storage applications, as presented in Table S1.† The CE-Py POP/SWCNT-AS nanocomposite incorporated within the device demonstrated a remarkable maximum energy density of 26.25 W h kg^{-1}, accompanied by a power density of 500 kW kg^{-1}, as elegantly illustrated in the Ragone plots (Fig. S5†). Notably, this energy density value stands in direct competition with recently documented SSC devices, such as PAQTA//PAQTA (18 W h kg^{-1}),[62] Fc-CMPs/rGO//Fc-CMPs/rGO (8 W h kg^{-1}),[63] and PANI/NCNT//PANI/NCNT (11.1 W h kg^{-1}).[64] EIS, electrochemical impedance spectroscopy, is a useful technique for describing electrode–electrolyte interfaces in a certain frequency range. The obtained fitted data are listed in Table S2.†

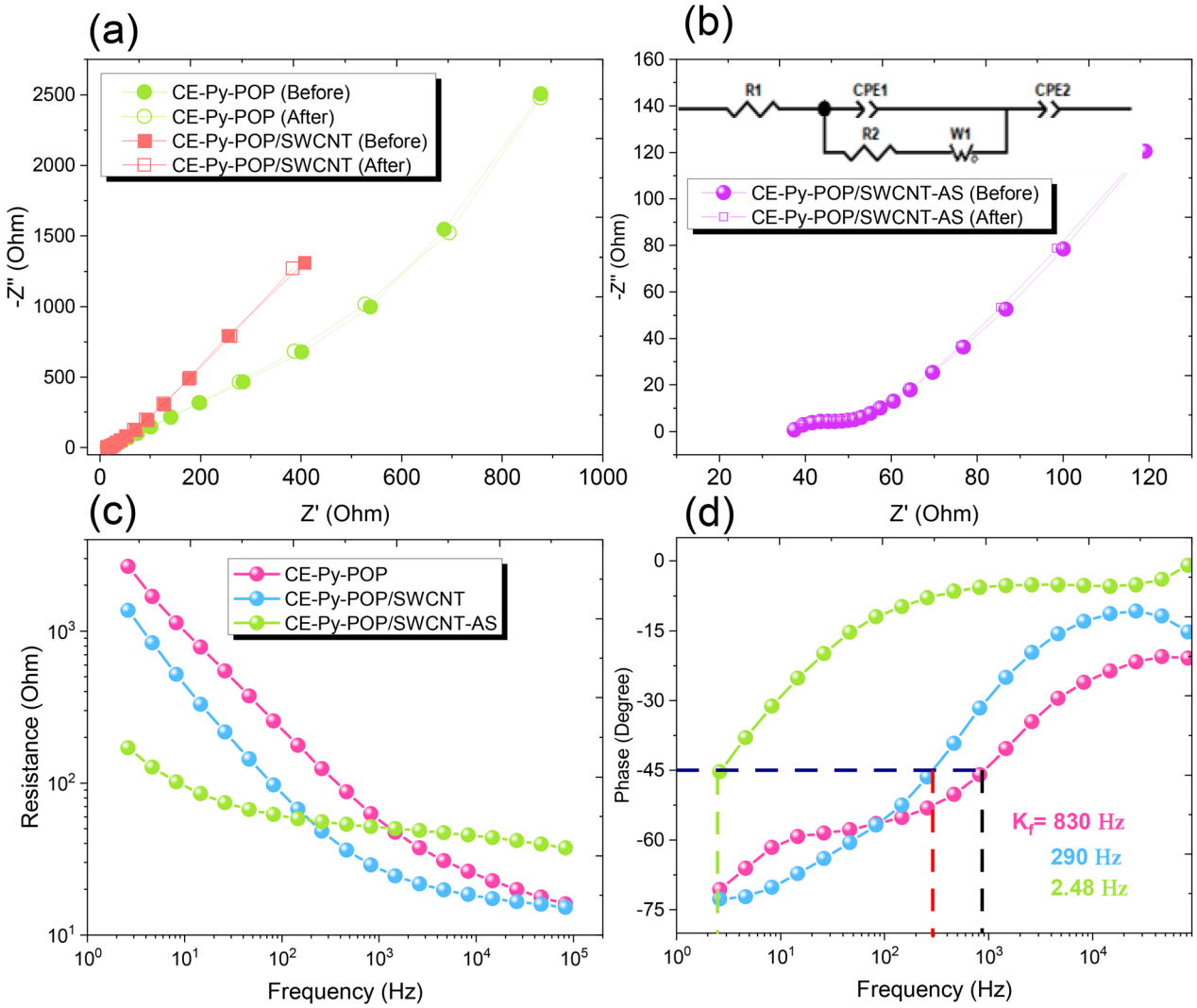

Fig. 7 Nyquist plot of (a) CE-Py POP, CE-Py POP/SWCNT, and (b) the CE-Py POP/SWCNT-AS (device) nanocomposite. (c) Bode plots of frequency-dependent resistance (magnitude) and (d) Bode plots of the frequency-dependent phase angle of CE-Py POP, CE-Py POP/SWCNT and CE-Py POP/SWCNT-AS (device) nanocomposite POPs.

Fig. 7(a) and (b) show the Nyquist plots of CE-Py POP, CE-Py POP/SWCNT, and CE-Py POP/SWCNT-AS (device) with an electrical equivalent circuit (inset), respectively. Based on the collected data, the CE-Py POP, CE-Py POP/SWCNT, and CE-Py POP/SWCNT-AS (device) provided measurements for the first series resistance, which is commonly referred to as the ohmic resistance, of 6.54, 5.60, and 39.13 Ω, respectively. Thus, the inclusion of SWCNT demonstrated the lowest resistance in CE-Py POP/SWCNT compared to that in CE-Py-POP, which as a result, provided the highest specific capacitance. The assembled two-electrode device has provided a significant value for series resistance. The charge transfer values for these electrodes were found to be 26.30, 10.43, and 76.80 Ω for CE-Py POP, CE-Py POP/SWCNT, and CE-Py POP/SWCNT-AS (device). Upon observation, the electrode employing SWCNT has delivered lower charge transfer compared to its CE-Py-POP counterpart. Furthermore, the charge transfer of the assembled device did not increase too much and delivered a moderate value of 76.80 Ω. In Fig. 7(c), the frequency-dependent magnitude Bode plots are depicted, showing lines characterized by a small resistance in the higher-frequency range and a negative slope in the lower-frequency region. Based on this knowledge, we inferred that all three of these porous materials will exhibit remarkable capacitive behavior when utilized as electrode materials for energy applications. In addition to this, Fig. 7(d) demonstrates frequency-dependent phase-angle Bode graphs for all three electrodes. The estimated knee frequencies were calculated based on the Nyquist plot. The knee frequency, which is typically attained when the phase angle reaches 45°, is a measure of an electrode material's rate performance. Both the capacitive and resistive characteristics become equal in such circumstances. The knee frequencies for CE-Py POP, CE-Py POP/SWCNT, and CE-Py POP/SWCNT-AS (device) were evaluated to be around 830, 290, and 2.48 Hz, respectively. As a result, all of the electrodes have exhibited a significant knee frequency indicating their potential when used as electrode materials in energy storage applications.[20,25,51,65–67]

Conclusions

We successfully synthesized a porous organic polymer containing CE-4NH_2 and Py monomers through Schiff base condensation and we named this polymer CE-Py POP. The CE-Py POP/SWCNT nanocomposite, formed by combining the CE-Py POP and SWCNTs, was evaluated for its suitability as an electrode material in supercapacitor devices. Compared to CE-Py POP, the CE-Py POP/SWCNT nanocomposite exhibited improved cycling stability, retaining 97.6% of its capacitance, and demonstrated a higher specific capacitance of 346 F g^{-1}. Our results demonstrate the potential of the CE-Py POP/SWCNT nanocomposite for higher-performance charge storage. This study introduces an innovative and straightforward approach involving π–π stacking interactions to create composite materials based on POPs. These composites exhibit exceptional performance in the field of energy storage.

Author contributions

Mohamed Gamal Mohamed: investigation, methodology, conceptualization, supervision, and writing – original draft. Wan-Chun Chang: investigation and methodology. Swetha V. Chaganti: investigation and writing – original draft. Santosh U. Sharma: investigation and writing – original draft. Jyh-Tsung Lee: supervision. Shiao-Wei Kuo: supervision.

Conflicts of interest

There are no conflicts to declare.

Acknowledgements

This study was supported financially by the Ministry of Science and Technology, Taiwan, under contracts NSTC 110-2124-M-002-013 and 111-2223-E-110-004. The authors thank the staff at National Sun Yat-sen University for their assistance with the TEM (ID: EM022600) experiments.

References

1 M. M. Samy, M. G. Mohamed, A. F. M. EL-Mahdy, T. H. Mansoure, K. C. W. Wu and S. W. Kuo, High-performance supercapacitor electrodes prepared from dispersions of tetrabenzonaphthalene-based conjugated microporous polymers and carbon nanotubes, *ACS Appl. Mater. Interfaces*, 2021, **13**, 51906–51916, DOI: **10.1021/acsami.1c05720**.

2 K. Yu, X. Pan, G. Zhang, X. Liao, X. Zhou, M. Yan, L. Xu and L. Mai, Nanowires in energy storage devices: structures, synthesis, and applications, *Adv. Energy Mater.*, 2018, **8**, 1802369, DOI: **10.1002/aenm.201802369**.

3 S. Y. Chang, A. M. Elewa, M. G. Mohamed, I. M. A. Mekhemer, M. M. Samy, K. Zhang, H. H. Chou and S. W. Kuo, Rational design and synthesis of bifunctional Dibenzo[g,p]chrysene-based conjugated microporous polymers for energy storage and visible light-driven photocatalytic hydrogen evolution, *Mater. Today Chem.*, 2023, **33**, 101680, DOI: **10.1016/j.mtchem.2023.101680**.

4 K. Li, H. Teng, Q. Sun, Y. Li, X. Wu, X. Dai, Y. Wang, S. Wang, Y. Zhang and K. Yao, Engineering active sites on nitrogen-doped carbon nanotubes/cobaltosic oxide heterostructure embedded in biotemplate for high-performance supercapacitors, *J. Energy Storage*, 2022, **53**, 105094, DOI: **10.1016/j.est.2022.105094**.

5 M. G. Mohamed, A. M. Elewa, M. S. Li and S. W. Kuo, Construction and multifunctional of hypercrosslinked porous organic polymers containing ferrocene unit for high-performance iodine adsorption and supercapacitor, *J. Taiwan Inst. Chem. Eng.*, 2023, **150**, 105045, DOI: **10.1016/j.jtice.2023.105045**.

6 J. Na, D. Zheng, J. Kim, M. Gao, A. Azhar, J. Lin and Y. Yamauchi, Material nanoarchitectonics of functional polymers and inorganic nanomaterials for smart supercapacitors, *Small*, 2022, **18**, 2102397, DOI: **10.1002/smll.202102397**.

7 S. M. Benoy, M. Pandey, D. Bhattacharjya and B. K. Saikia, Recent trends in supercapacitor-battery hybrid energy storage devices based on carbon materials, *J. Energy Storage*, 2022, **52**, 104938, DOI: **10.1016/j.est.2022.104938**.

8 K. Li, Z. Hu, R. Zhao, J. Zhou, C. Jing, Q. Sun, J. Rao, K. Yao, B. Dong, X. Liu, H. Li, Y. Zhang and J. Ji, A multidimensional rational design of nickel–iron sulfide and carbon nanotubes on diatomite via synergistic modulation strategy for supercapacitors, *J. Colloid Interface Sci.*, 2021, **603**, 799–809, DOI: **10.1016/j.jcis.2021.06.131**.

9 I. K. Moon, B. Ki and J. Oh, Three-dimensional porous stretchable supercapacitor with wavy structured PEDOT: PSS/graphene electrode, *Chem. Eng. J.*, 2020, **392**, 123794, DOI: **10.1016/j.cej.2019.123794**.

10 X. Lu, J. Wang, T. Li, B. Ding, S. Liu, J. Henzie, M. A. Amin, B. Yuliarto, Y. Sugahara and Y. Yamauchi, N-doped hollow carbon nanoplates with mesoporous thin shells towards high-performance supercapacitors, *J. Power Sources*, 2022, **542**, 231776, DOI: **10.1016/j.jpowsour.2022.231776**.

11 Y. He, T. Zhuang, S. Ruan, X. Xia, J. Zhang, H. Huang, Y. Gan and W. Zhang, An innovative poly(ionic liquid) hydrogel-based anti-freezing electrolyte with high conductivity for supercapacitor, *Chem. Eng. J.*, 2023, **466**, 143209, DOI: **10.1016/j.cej.2023.143209**.

12 A. O. Mousa, C. H. Chuang, S. W. Kuo and M. G. Mohamed, Strategic Design and Synthesis of Ferrocene Linked Porous Organic Frameworks toward Tunable CO_2 Capture and Energy Storage, *Int. J. Mol. Sci.*, 2023, **24**, 12371, DOI: **10.3390/ijms241512371**.

13 P. N. Singh, M. G. Mohamed, S. V. Chaganti, S. U. Sharma, M. Ejaz, J. T. Lee and S. W. Kuo, Rational Design of Ultrastable Conjugated Microporous Polymers Based on Pyrene and Perylene Units as High-Performance Organic Electrode Materials for Supercapacitor Applications, *ACS Appl. Energy Mater.*, 2023, **6**, 8277–8287, DOI: **10.1021/acsaem.3c01391**.

14 Y. Wang, W. Li, L. Zhang, X. Zhang, B. Tan, J. Hao, J. Zhang, X. Wang, Q. Hu and X. Lu, Amorphous cobalt hydrogen phosphate nanosheets with remarkable electrochemical performances as advanced electrode for supercapacitors, *J. Power Sources*, 2020, **449**, 227487, DOI: **10.1016/j.jpowsour.2019.227487**.

15 A. O. Mousa, Z. I. Lin, C. H. Chuang, C. K. Chen, S. W. Kuo and M. G. Mohamed, Rational Design of Bifunctional Microporous Organic Polymers Containing Anthracene and Triphenylamine Units for Energy Storage and Biological Applications, *Int. J. Mol. Sci.*, 2023, **24**, 8966, DOI: **10.3390/ijms24108966**.

16 M. G. Mohamed, S. V. Chaganti, M. S. Li, M. M. Samy, S. U. Sharma, J. T. Lee, M. H. Elsayed, H. H. Chou and S. W. Kuo, Ultrastable porous organic polymers containing thianthrene and pyrene units as organic electrode materials for supercapacitors, *ACS Appl. Energy Mater.*, 2022, **5**, 6442–6452, DOI: **10.1021/acsaem.2c00942**.

17 Y. S. Ye, M. G. Mohamed, W. C. Chen and S. W. Kuo, Integrating the multiple functionalities in metalloporphyrin porous organic polymers enabling strong polysulfide anchoring and rapid electrochemical kinetics in Li–S batteries, *J. Mater. Chem. A*, 2023, **11**, 9112–9124, DOI: **10.1039/D2TA09232H**.

18 T. Zhang, G. Xing, W. Chen and L. Chen, Porous organic polymers: a promising platform for efficient photocatalysis, *Mater. Chem. Front.*, 2022, **4**, 332–353, DOI: **10.1039/C9QM00633H**.

19 W. Song, Y. Zhang, C. H. Tran, H. K. Choi, D. G. Yu and I. Kim, Porous organic polymers with defined morphologies: synthesis, assembly, and emerging applications, *Prog. Polym. Sci.*, 2023, **142**, 101691, DOI: **10.1016/j.progpolymsci.2023.101691**.

20 M. M. Samy, S. U. Sharma, M. G. Mohamed, A. A. K. Mohammed, S. V. Chaganti, J. T. Lee and S. W. Kuo, Conjugated microporous polymers containing ferrocene units for high carbon dioxide uptake and energy storage, *Mater. Chem. Phys.*, 2022, **287**, 126177, DOI: **10.1016/j.matchemphys.2022.126177**.

21 M. G. Mohamed, T. H. Mansoure, Y. Takashi, M. M. Samy, T. Chen and S. W. Kuo, Ultrastable porous organic/inorganic polymers based on polyhedral oligomeric silsesquioxane (POSS) hybrids exhibiting high performance for thermal property and energy storage, *Microporous Mesoporous Mater.*, 2021, **328**, 111505, DOI: **10.1016/j.micromeso.2021.111505**.

22 A. O. Mousa, M. G. Mohamed, C. H. Chuang and S. W. Kuo, Carbonized Aminal-Linked Porous Organic Polymers Containing Pyrene and Triazine Units for Gas Uptake and Energy Storage, *Polymer*, 2023, **15**, 1891, DOI: **10.3390/polym15081891**.

23 K. I. Aly, M. M. Sayed, M. G. Mohamed, S. W. Kuo and O. Younis, A facile synthetic route and dual function of network luminescent porous polyester and copolyester containing porphyrin moiety for metal ions sensor and dyes adsorption, *Microporous Mesoporous Mater.*, 2020, **298**, 110063, DOI: **10.1016/j.micromeso.2020.110063**.

24 M. G. Mohamed, S. U. Sharma, N. Y. Liu, T. H. Mansoure, M. M. Samy, S. V. Chaganti, Y. L. Chang, J. T. Lee and S. W. Kuo, Ultrastable covalent triazine organic framework based on anthracene moiety as platform for high-performance carbon dioxide adsorption and supercapacitors, *Int. J. Mol. Sci.*, 2022, **23**, 3174, DOI: **10.3390/ijms23063174**.

25 M. Ejaz, M. G. Mohamed, S. U. Sharma, J. T. Lee, C. F. Huang, T. Chen and S. W. Kuo, An Ultrastable Porous Polyhedral Oligomeric Silsesquioxane/Tetraphenylthiophene Hybrid as a High-Performance Electrode for Supercapacitors, *Molecules*, 2022, **27**, 6238, DOI: **10.3390/molecules27196238**.

26 C. Zhang, Y. He, P. Mu, X. Wang, Q. He, Y. Chen, J. Zeng, F. Wang, Y. Xu and J. X. Jiang, Toward high performance

thiophene–containing conjugated microporous polymer anodes for lithium–ion batteries through structure design, *Adv. Funct. Mater.*, 2018, **28**, 1705432, DOI: **10.1002/adfm.201705432**.

27 M. M. Samy, I. M. A. Mekhemer, M. G. Mohamed, M. H. Elsayed, K. H. Lin, Y. K. Chen, T. L. Wu, H. H. Chou and S. W. Kuo, Conjugated microporous polymers incorporating Thiazolo[5,4-d]thiazole moieties for Sunlight-Driven hydrogen production from water, *Chem. Eng. J.*, 2022, **446**, 137158, DOI: **10.1016/j.cej.2022.137158**.

28 L. Y. Wen, Y. Mi, C. L. Wang, Y. G. Fang, F. Grote, H. P. Zhao, M. Zhou and Y. Lei, Cost–effective atomic layer deposition synthesis of Pt nanotube arrays: application for high performance supercapacitor, *Small*, 2014, **10**, 3162–3168, DOI: **10.1002/smll.201400436**.

29 M. M. Samy, M. G. Mohamed, S. U. Sharma, S. V. Chaganti, T. H. Mansoure, J. T. Lee, T. Chen and S. W. Kuo, Constructing conjugated microporous polymers containing triphenylamine moieties for high-performance capacitive energy storage, *Polymer*, 2023, **264**, 125541, DOI: **10.1016/j.polymer.2022.125541**.

30 J. Zhang, H. Zhao, J. Li, H. Jin, X. Yu, Y. Lei and S. Wang, In situ encapsulation of iron complex nanoparticles into biomass–derived heteroatom–enriched carbon nanotubes for high–performance supercapacitors, *Adv. Energy Mater.*, 2019, **9**, 1803221, DOI: **10.1002/aenm.201803221**.

31 L. Mei, X. Cui, Q. Duan, Y. Li, X. Lv and H. G. Wang, Metal phthalocyanine-linked conjugated microporous polymer hybridized with carbon nanotubes as a high-performance flexible electrode for supercapacitors, *Int. J. Hydrogen Energy*, 2020, **45**, 22950–22958, DOI: **10.1016/j.ijhydene.2020.06.208**.

32 F. Ran, X. Yang, X. Xu, Y. Bai and L. Shao, Boosting the charge storage of layered double hydroxides derived from carbon nanotube-tailored metal organic frameworks, *Electrochim. Acta*, 2019, **301**, 117–125, DOI: **10.1016/j.electacta.2019.01.142**.

33 C. Sengottaiyan, R. Jayavel, R. G. Shrestha, T. Subramani, S. Maji, J. H. Kim, J. P. Hill, K. Ariga and L. K. Shrestha, Indium oxide/carbon nanotube/reduced graphene oxide ternary nanocomposite with enhanced electrochemical supercapacitance, *Bull. Chem. Soc. Jpn.*, 2019, **92**, 521–528, DOI: **10.1246/bcsj.20180338**.

34 M. M. Samy, M. G. Mohamed and S. W. Kuo, Pyrene-functionalized tetraphenylethylene polybenzoxazine for dispersing single-walled carbon nanotubes and energy storage, *Compos. Sci. Technol.*, 2020, **199**, 108360, DOI: **10.1016/j.compscitech.2020.108360**.

35 L. Lu, S. Xu, J. An and S. Yan, Electrochemical performance of CNTs/RGO/MnO_2 composite material for supercapacitor, *Nanomater. Nanotechnol.*, 2016, **6**, 1–7, DOI: **10.1177/1847980416663687**.

36 Y. Zhang, Z. Bi, Y. Liang, W. Zuo, G. Xu and M. Zhu, Ultrahigh line-capacity and flexible graphene/carbon nanotube/tin oxide fibers as sodium ion battery anodes, *Energy Storage Mater.*, 2022, **48**, 35–43, DOI: **10.1016/j.ensm.2022.03.002**.

37 R. R. Salunkhe, J. Lin, V. Malgras, S. X. Dou, J. H. Kim and Y. Yamauchi, Large-scale synthesis of coaxial carbon nanotube/$Ni(OH)_2$ composites for asymmetric supercapacitor application, *Nano Energy*, 2015, **11**, 211–218, DOI: **10.1016/j.nanoen.2014.09.030**.

38 C. Lei, Y. Yehui, O. Raphael, Y. Meltem, H. Jin, L. Jian, L. Yong and Z. Xiangwu, Carbon materials dedicate to bendable supports for flexible lithium-sulfur batteries, *Energy Storage Mater.*, 2023, 102817, DOI: **10.1016/j.ensm.2023.102817**.

39 J. Li, W. Lu, Y. Yan and T. W. Chou, High performance solid-state flexible supercapacitor based on Fe_3O_4/carbon nanotube/polyaniline ternary films, *J. Mater. Chem. A*, 2017, **5**, 11271–11277, DOI: **10.1039/C7TA02008B**.

40 M. G. Mohamed, W. C. Chang and S. W. Kuo, Crown ether- and benzoxazine-linked porous organic polymers displaying enhanced metal ion and CO_2 capture through solid-state chemical transformation, *Macromolecules*, 2022, **55**, 7879–7892, DOI: **10.1021/acs.macromol.2c01216**.

41 Y. Xiong, T. Ge, L. Xu, L. Wang, J. He, X. Zhou, Y. Tian and Z. Zhao, A fundamental study on selective extraction of Li^+ with dibenzo-14-crown-4 ether: toward new technology development for lithium recovery from brines, *J. Environ. Manage.*, 2022, **310**, 114705, DOI: **10.1016/j.jenvman.2022.114705**.

42 H. Zhao, J. Qi, X. Tang, K. Zhang, J. Teng, H. Ding, Q. Tao and J. Li, Effect of crown ether additive on the compatibility of electrolyte and hard carbon anode in sodium ion battery, *J. Alloys Compd.*, 2023, **948**, 169823, DOI: **10.1016/j.jallcom.2023.169823**.

43 M. G. Mohamed and S. W. Kuo, Crown ether-functionalized polybenzoxazine for metal ion adsorption, *Macromolecules*, 2020, **53**, 2420–2429, DOI: **10.1021/acs.macromol.9b02519**.

44 S. An, C. Lu, Q. Xu, C. Lian, C. Peng, J. Hu, X. Zhuang and H. Liu, Constructing catalytic crown ether-based covalent organic frameworks for electroreduction of CO_2, *ACS Energy Lett.*, 2021, **6**, 3496–3502, DOI: **10.1021/acsenergylett.1c01681**.

45 L. Yuan, J. Zhu, S. Wu and C. Chi, Enhanced emission by stacking of crown ether side chains in a 2D covalent organic framework, *Chem. Commun.*, 2022, **58**, 1302–1305, DOI: **10.1039/D1CC03409J**.

46 M. Boota, C. Chen, M. Bécuwe, L. Miao and Y. Gogotsi, Pseudocapacitance and excellent cyclability of 2, 5-dimethoxy-1, 4-benzoquinone on graphene, *Energy Environ. Sci.*, 2016, **9**, 2586–2594, DOI: **10.1039/C6EE00793G**.

47 M. G. Mohamed, S. Y. Chang, M. Ejaz, M. M. Samy, A. O. Mousa and S. W. Kuo, Design and Synthesis of Bisulfone-Linked Two-Dimensional Conjugated Microporous Polymers for CO_2 adsorption and Energy Storage, *Molecules*, 2023, **28**, 3234, DOI: **10.3390/molecules28073234**.

48 C. Su, H. He, L. Xu, K. Zhao, C. Zheng and C. Zhang, A mesoporous conjugated polymer based on a high free radical density polytriphenylamine derivative: its prepa-

ration and electrochemical performance as a cathode material for Li-ion batteries, *J. Mater. Chem. A*, 2017, **5**, 2701–2709, DOI: **10.1039/C6TA10127E**.

49 X. Liu, C. Ma, Y. Wen, X. Chen, X. Zhao, T. Tang, R. Holze and E. Mijowska, Highly efficient conversion of waste plastic into thin carbon nanosheets for superior capacitive energy storage, *Carbon*, 2021, **171**, 819–828, DOI: **10.1016/j.carbon.2020.09.057**.

50 X. Shan, K. Song, S. Huang, J. Wang, F. Shi and D. Zhao, Novel porous nitrogen-doped carbon composite with CNTs/Cu-Ni as high-performance supercapacitor electrode, *J. Electroanal. Chem.*, 2022, **920**, 116610, DOI: **10.1016/j.jelechem.2022.116610**.

51 F. Rafik, H. Gualous, R. Gallay, A. Crausaz and A. Berthon, Frequency, thermal and voltage supercapacitor characterization and modeling, *J. Power Sources*, 2007, **165**, 928–934, DOI: **10.1016/j.jpowsour.2006.12.021**.

52 Y. Xu, S. Wang, H. Peng, Z. Yang, D. J. Martin, A. Bund, A. K. Nanjundan and Y. Yamauchi, Electrochemical characteristics of cobaltosic oxide in organic electrolyte according to bode plots: double-layer capacitance and pseudocapacitance, *ChemElectroChem*, 2019, **6**, 2456–2463, DOI: **10.1002/celc.201900289**.

53 K. C. S. Lakshmi and B. Vedhanarayanan, High-performance supercapacitors: a comprehensive review on paradigm shift of conventional energy storage devices, *Batteries*, 2023, **9**, 202, DOI: **10.3390/batteries9040202**.

54 M. Ejaz, M. G. Mohamed and S. W. Kuo, Solid state chemical transformation provides a fully benzoxazine-linked porous organic polymer displaying enhanced CO_2 capture and supercapacitor performance, *Polym. Chem.*, 2023, **14**, 2494–2509, DOI: **10.1039/D3PY00158J**.

55 Y. Li, S. Zheng, X. Liu, P. Li, L. Sun, R. Yang, S. Wang, Z. S. Wu, X. Bao and W. Q. Deng, Conductive microporous covalent triazine–based framework for high–performance electrochemical capacitive energy storage, *Angew. Chem., Int. Ed.*, 2018, **57**, 7992–7996, DOI: **10.1002/ange.201711169**.

56 F. Hu, J. Wang, S. Hu, L. Li, W. Shao, J. Qiu, Z. Lei, W. Deng and X. Jian, Engineered fabrication of hierarchical frameworks with tuned pore structure and N, O-co-doping for high-performance supercapacitors, *ACS Appl. Mater. Interfaces*, 2017, **9**, 31940–31949, DOI: **10.1021/acsami.7b09801**.

57 A. M. Khattak, Z. A. Ghazi, B. Liang, N. A. Khan, A. Iqbal, L. Li and Z. Tang, A redox-active 2D covalent organic framework with pyridine moieties capable of faradaic energy storage, *J. Mater. Chem. A*, 2016, **4**, 16312–16317, DOI: **10.1039/C6TA05784E**.

58 M. Ejaz, M. G. Mohamed, W. C. Chang and S. W. Kuo, Synthesis and design of hypercrosslinked porous organic frameworks containing tetraphenylpyrazine unit for high-performance supercapacitor, *J. Polym. Sci.*, 2023, DOI: **10.1002/pol.20230174**.

59 M. G. Mohamed, H. Y. Hu, M. Madhu, M. M. Samy, I. M. A. Mekhemer, W. L. Tseng, H. H. Chou and S. W. Kuo, Ultrastable Two-Dimensional Fluorescent Conjugated Microporous Polymers Containing Pyrene and Fluorene Units for Metal Ion Sensing and Energy Storage, *Eur. Polym. J.*, 2023, **189**, 111980, DOI: **10.1016/j.eurpolymj.2023.111980**.

60 M. G. Mohamed, X. Zhang, T. H. Mansoure, A. F. M. El-Mahdy, C. F. Huang, M. Danko, Z. Xin and S. W. Kuo, Hypercrosslinked porous organic polymers based on tetraphenylanthraquinone for CO_2 uptake and high-performance supercapacitor, *Polymer*, 2020, **205**, 122857, DOI: **10.1016/j.polymer.2020.122857**.

61 M. G. Mohamed, H. Y. Hu, M. Madhu, M. Ejaz, S. U. Sharma, W. L. Tseng, M. M. Samy, C. W. Huang, J. T. Lee and S. W. Kuo, Construction of Ultrastable Conjugated Microporous Polymers Containing Thiophene and Fluorene for Metal Ion Sensing and Energy Storage, *Micromachines*, 2022, **13**, 1466, DOI: **10.3390/mi13091466**.

62 L. Liao, H. Wang, M. Zhu and A. Thomas, Efficient Supercapacitor Energy Storage using Conjugated Microporous Polymer Networks Synthesized from Buchwald–Hartwig Coupling, *Adv. Mater.*, 2018, **30**, 1705710, DOI: **10.1002/adma.201705710**.

63 A. M. Khattak, H. Sin, Z. A. Ghazi, X. He, B. Liang, N. A. Khan, H. R. Alanagh, A. Iqbal, L. Li and Z. Tang, Controllable Fabrication of Redox-Active Conjugated Microporous Polymers on Reduced Graphene Oxide for High Performance Faradaic Energy Storage, *J. Mater. Chem. A*, 2018, **6**, 18827–18832, DOI: **10.1039/c8ta07913g**.

64 R. Malik, L. Zhang, C. McConnell, M. Schott, Y. Y. Hsieh, R. Noga, N. T. Alvarez and V. Shanov, Three-Dimensional, Free-Standing Polyaniline/Carbon Nanotube Composite-based Electrode for High-Performance Supercapacitors, *Carbon*, 2017, **116**, 579–590, DOI: **10.1016/j.carbon.2017.02.036**.

65 M. G. Mohamed, S. V. Chaganti, S. U. Sharma, M. M. Samy, M. Ejaz, J. T. Lee, K. Zhang and S. W. Kuo, Constructing Conjugated Microporous Polymers Containing the Pyrene-4, 5, 9, 10-Tetraone Unit for Energy Storage, *ACS Appl. Energy Mater.*, 2022, **5**, 10130–10140, DOI: **10.1021/acsaem.2c01842**.

66 T. H. Weng, M. G. Mohamed, S. U. Sharma, S. V. Chaganti, M. M. Samy, J. T. Lee and S. W. Kuo, Ultrastable three-dimensional triptycene-and tetraphenylethene-conjugated microporous polymers for energy storage, *ACS Appl. Energy Mater.*, 2022, **5**, 14239–14249, DOI: **10.1021/acsaem.2c02809**.

67 M. G. Mohamed, M. M. Samy, T. H. Mansoure, S. U. Sharma, M. S. Tsai, J. H. Chen, J. T. Lee and S. W. Kuo, Dispersions of 1,3,4-Oxadiazole-Linked Conjugated Microporous Polymers with Carbon Nanotubes as a High-Performance Electrode for Supercapacitors, *ACS Appl. Energy Mater.*, 2022, **5**, 3677–3688, DOI: **10.1021/acsaem.2c00100**.